Towards Stabilized and Efficient Diffusion Transformers through Long-Skip-Connections with Spectral Constraints

Guanjie Chen^{1*} Xinyu Zhao^{2*} Yucheng Zhou³ Xiaoye Qu ⁴ Tianlong Chen ^{2†} Yu Cheng^{5†}

¹Shanghai Jiao Tong University ²The University of North Carolina at Chapel Hill ³SKL-IOTSC, CIS, University of Macau ⁴Huazhong University of Science and Technology ⁵The Chinese University of Hong Kong

chenguanjie@sjtu.edu.cn, xinyu@cs.unc.edu

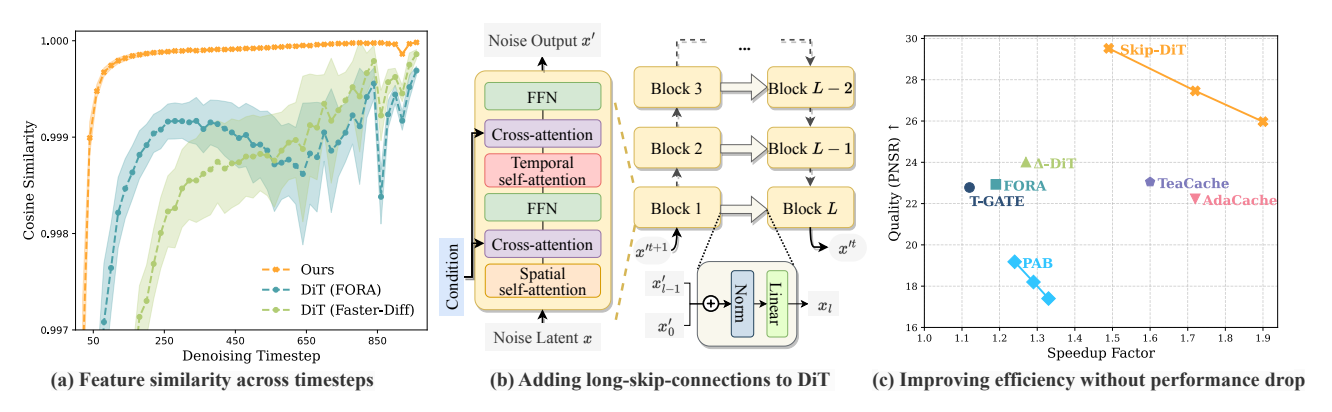


Figure 1. (a) Feature similarities between standard and cache-accelerated outputs in vanilla DiT (caching with FORA [30] and Faster-Diff [13]) and our proposed Skip-DiT. Skip-DiT presents consistently higher feature similarity, demonstrating superior stability after caching. (b) Illustration of Skip-DiT that modifies vanilla DiT models using long-skip-connection to connect shallow and deep DiT blocks. Dashed arrows indicate paths where computation can be skipped in cached inference. (c) Comparison of video generation quality (PNSR) and inference speedup of different DiT caching methods. Skip-DiT maintains higher generation quality even at greater speedup factors.

Abstract

Diffusion Transformers (DiT) have emerged as a powerful architecture for image and video generation, offering superior quality and scalability. However, their practical application suffers from inherent dynamic feature instability, leading to error amplification during cached inference. Through systematic analysis, we identify the absence of longrange feature preservation mechanisms as the root cause of unstable feature propagation and perturbation sensitivity. To this end, we propose Skip-DiT, an image and video generative DiT variant enhanced with Long-Skip-Connections (LSCs) - the key efficiency component in U-Nets. Theoretical spectral norm and visualization analysis demonstrate how LSCs stabilize feature dynamics. Skip-DiT architecture and its stabilized dynamic feature enable an efficient statical caching mechanism that reuses deep features across timesteps while updating shallow components. Extensive experiments across the image and video generation tasks demonstrate that Skip-DiT achieves: (1) 4.4× training

acceleration and faster convergence, (2) $1.5-2\times$ inference acceleration with negligible quality loss and high fidelity to the original output, outperforming existing DiT caching methods across various quantitative metrics. Our findings establish Long-Skip-Connections as critical architectural components for stable and efficient diffusion transformers. Codes are provided in the URL¹.

1. Introduction

Diffusion models [3, 8, 24, 48] have emerged as the de-facto solution for visual generation, owing to their high fidelity outputs and ability to incorporate various conditioning signals, particularly natural language. Classical diffusion models typically adopt U-Net [27] as their denoising backbone.

Recently, Diffusion Transformers (DiT) [4, 23] introduce an alternative architecture to replace traditional convolu-

¹https://github.com/OpenSparseLLMs/Skip-DiT

^{*}Equal Contribution.

[†]Corresponding Authors.

tional networks with Vision Transformers, offering enhanced scalability potential. While initially designed for image generation, DiT has demonstrated remarkable effectiveness when extended to video generation tasks [14, 18, 25]. Despite these advances, DiT still faces challenges in practical deployment due to its slow convergence rates [20, 41, 49] and substantial inference time requirements, posing significant constraints on training efficiency and real-time applications.

Numerous approaches have been proposed to improve the efficiency of diffusion models, including reduced sampling techniques [33], distillation methods [29, 42], and quantization strategies [5]. Among these approaches, caching has emerged as one of the most effective strategies for enhancing inference efficiency, owing to its low computational cost while maintaining high fidelity and similarity to the original models through efficient feature reuse [6, 11, 16, 30, 46, 50]. However, existing caching methods in DiT still face challenges in visual generation. DiT architecture exhibits significant sample-wise variation in caching function responses, requiring adaptive per-sample hyperparameter tuning and introducing computational overhead [11, 16]. Besides, current caching methods still yield suboptimal generative results with visible artifacts when cached with larger intervals [6, 11, 30, 50], suggesting error amplification in DiT's transformer blocks. Besides, the training efficiency gap further compounds these challenges. DiT is shown to converge more slowly in training [41, 49], and the reasons remain unexplained from architectural perspectives.

DiT efficiency is hindered by the above challenges, but U-Net-based diffusion models can leverage their Long-Skip-Connections (LSCs) to extend cache intervals without complex timestep scheduling or severe performance degradation [13, 17]. The LSCs not only make caching stable and robust during inference, but they have also been proven as the key factor for stabilizing training and accelerating convergence for U-Net-based diffusion models [9]. These observations lead to our core research question:

(Q) What are the architectural root causes of feature instability and inefficiency in DiT, and to what extent can Long-Skip-Connections mitigate these issues while preserving generation quality?

In this study, we systematically analyze the feature distribution in DiT: • We conduct a preliminary experiment that incorporates Long-Skip-Connections (LSCs) with DiT, and visualize the dynamic features of DiT with and without LSCs by adding perturbations in parameters and model inputs, the feature similarity landscape and plots validate the instability of vanilla DiT (w/o LSCs), which we formally characterize as *Dynamic Feature Instability*, indicating an uncontrolled spectral norm that affects both statistical stability, model robustness, and convergence rate. • We then theoretically

prove the superior stability and robustness of DiT with LSCs over vanilla DiT via spectral analysis

To this end, we propose the Long-Skip-Connected-DiT, namely Skip-DiT, a DiT architecture that employs spectral constraints—limiting the maximum singular value of weight matrices to ensure stable gradient flow and reduced sensitivity to perturbations. By incorporating these constraints through LSCs, our approach provides theoretical feature stability guarantees and enhanced efficiency in both training and inference, validated through quantitative experiments and visual analysis. The LSCs also enable output caching of stabilized features from deep blocks, requiring the computation of only shallow blocks during inference at statically chosen caching timesteps.

To evaluate our proposed Skip-DiT, we conduct extensive experiments across 3 DiT backbones, assess training performance on 6 models, and inference efficiency on 7 visual generation tasks, spanning both class and text conditional image/video generation. Skip-DiT achieves superior training efficiency while consistently outperforming both standard baselines and prior caching methods in qualitative and quantitative evaluations. To summarize, we claim the following contribution of this work:

- Through theoretical analysis and comprehensive visualization, we identify *Dynamic Feature Instability* as a fundamental root cause that impairs DiT training efficiency and hinders effective inference acceleration.
- We introduce Skip-DiT, an enhanced DiT architecture incorporating Long-Skip-Connections between shallow and deep transformer blocks. Our approach provides theoretical guarantees for feature stability through spectral norm analysis and enables efficient feature caching at strategically selected timesteps.
- We conduct extensive evaluations across different DiT base models, and various image and video generation benchmarks. Results of substantial training and inference speedup and nearly undamaged generation quality consistently endorse the effectiveness of Skip-DiT. For example, compared to vanilla DiT, Skip-DiT achieves up to 4.4× training acceleration with even better generation quality. When compared to state-of-the-art DiT caching techniques, Skip-DiT delivers 1.5-2× additional speedup while maintaining superior output fidelity.

2. Related Works

Transformer-based Diffusion Models The diffusion model has become the dominating architecture for image and video generation, whose main idea is iterative generate high-fidelity images or video frames from noise [26]. Early diffusion models mainly employ U-Net as their denoising backbone [3, 24]. However, U-Net architectures struggle to model long-range dependencies due to the local nature of convolutions. Researchers proposing diffusion

transformer model (DiT) for image generation [2, 4, 23]. Recent years have witnessed a significant growth in studies of video DiT. Proprietary DiT such as Sora [20] and Movie-Gen [25] show impressive generation quality, also evidenced by open-sourced implementation [12, 51]. Latte decomposes the spatial and temporal dimensions into four efficient variants for handling video tokens, allowing effective modeling of the substantial number of tokens extracted from videos in the latent space [18]. CogvideoX adds a 3D VAE combined with an expert transformer using adaptive LayerNorm, which enables the generation of longer, high-resolution videos [40].

Diffusion Acceleration with Feature Caching Since the diffusion model involves iterative denoising, caching features across time-steps, model layers, and modules has been found an effective way to save inference computation costs. For U-Net Diffusion, DeepCache [17] and FRDiff [32] exploit temporal redundancy by reusing features across adjacent denoising steps. While other works take a more structured approach by analyzing and caching specific architectural components–Faster Diffusion [13] specifically targets encoder feature reuse while enabling parallel decoder computation, and Block Caching [38] introduces automated caching schedules for different network blocks based on their temporal stability patterns. Recently, cache-based acceleration has also been applied to DiT. PAB [50] introduces a pyramid broadcasting strategy for attention outputs. Δ -DiT [6] proposes adaptive caching of different DiT blocks based on their roles in a generation-rear blocks during early sampling for details and front blocks during later stages for outlines. T-Gate [47] identifies a natural two-stage inference process, enabling the caching and reuse of text-oriented semantic features after the initial semantics-planning stage. To deal with the sample-wise variation in DiT, adaptive caching methods like AdaCache [11] and TeaCache [16] are proposed to predict the feature distribution according to the input.

3. Methodology

3.1. Preliminaries

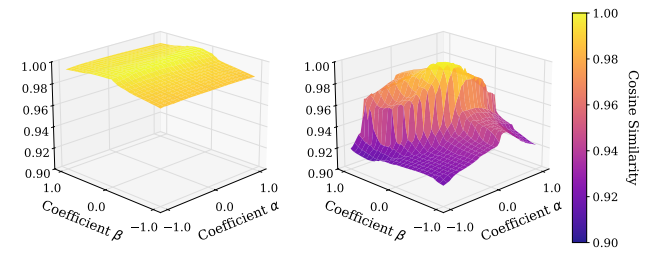
Diffusion model The concept of diffusion models mirrors particle dispersion physics, where particles spread out with random motion. It involves forward and backward diffusion. The forward phase adds noise to data across T timesteps. Starting from data $\mathbf{x}_0 \sim q(\mathbf{x})$, noise is added to the data at each timestep $t \in \{1 \dots T\}$.

$$\mathbf{x}_t = \sqrt{\alpha_t} \mathbf{x}_{t-1} + \sqrt{1 - \alpha_t} \epsilon_{t-1} \tag{1}$$

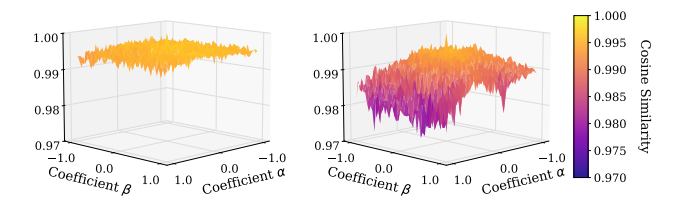
where α determines noise level while $\epsilon \sim \mathcal{N}(0,\mathbf{I})$ represents Gaussian noise. The data \mathbf{x}_t becomes increasingly noisy with time, reaching $\mathcal{N}(0,\mathbf{I})$ at t=T. Reverse diffusion then reconstructs the original data as follows, where μ_{θ} and Σ_{θ} refer to the learnable mean and covariance:

$$p_{\theta}(\mathbf{x}_{t-1}|\mathbf{x}_t) = \mathcal{N}(\mathbf{x}_{t-1}; \mu_{\theta}(\mathbf{x}_t, t), \Sigma_{\theta}(\mathbf{x}_t, t)), \quad (2)$$

Diffusion Transformer In our study, we consider two types of DiT models processing different visual information: image DiT and video DiT. • Image DiT model follows Vision Transformer, each block contains self-attention, crossattention, and feed-forward networks (FFN), where the crossattention module incorporates text and timestep conditions. • Video DiT adopts dual-subblock architecture: the spatial Transformer subblock processes tokens within the same time frame, while the temporal subblock manages cross-frame relationships. These blocks alternate in sequence, with crossattention integrating conditional inputs. A complete video DiT block pairs one spatial and one temporal component in an interleaved pattern, following [18, 50].



(a) Feature similarity landscape on class-to-image task.



(b) Feature similarity landscape on text-to-video task.

Figure 2. Feature stability comparison between Skip-DiT (left) and vanilla DiT (right) on class-to-image (DiT-XL) and text-to-video (Latte) generation. We inject perturbations δ (magnitudes α) and η (magnitudes β), normalized with specific coefficients ($\epsilon=1e^{-3}$ for DiT-XL and $2e^{-2}$ for Latte), then measure the similarity between the standard and perturbed features.

3.2. Dynamic Feature Instability in DiT

DiT models are known to suffer from low training efficiency [49] and unstable feature distributions during inference [11, 16], posing significant challenges for acceleration. This contrasts sharply with U-Net [27] architectures where Long-Skip-Connections (LSCs) enhance training stability and efficiency [9], and enable simple but reliable acceleration through feature reuse [13, 17]. To explore this architectural discrepancy, we integrate LSCs into DiT-XL [22] as in Figure 2 (b) and train from scratch as the preliminary experiment. Training settings is the same as in Section 4.1

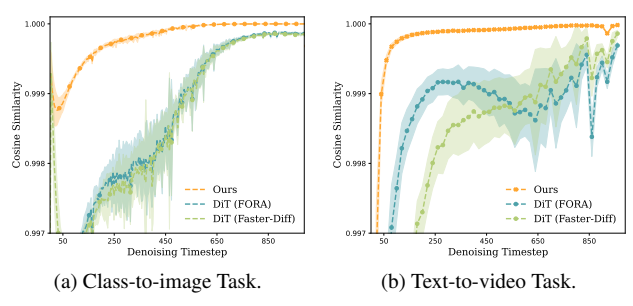


Figure 3. Comparison between standard and cache-accelerated outputs in vanilla DiT versus Skip-DiT, with Latte (text-to-video generation) and DiT-XL (class-to-image generation) serving as base architectures. Both mean and standard deviation across samples are shown. Vanilla DiT exhibits much higher sample variance.

Visualizing Feature Stability of DiT Let $\theta \in \mathbb{R}^d$ denote the original parameters of model $f(x;\theta)$. Given random perturbation vectors $\delta, \eta \in \mathbb{R}^d$, $\|\delta\| = \|\eta\| = \epsilon \|\theta\|$, with $0 < \epsilon < 1$ which is normalization coefficient. we construct perturbed parameters: $\theta' = \theta + \alpha\delta + \beta\eta$, where $\alpha, \beta \in \mathbb{R}$ control perturbation magnitudes. The feature stability landscape for 3D visualization is defined as:

$$L(\alpha, \beta) = \text{CosineSimilarity}(f(x; \theta), f(x; \theta'))$$
 (3)

To visualize the feature stability across timesteps, we perturb the inputs with cached values, following the caching strategy of FORA[30] and FasterDiff[41], and we take cosine similarity to measure the distance with and without caching. Visualized results are illustrated in Figure 2(a) and 3(a).

Dynamic Feature Instability Our preliminary experiments and visualizations reveal that vanilla DiT models exhibit significant sensitivity to perturbations in both parameters and input features, with feature similarity across timesteps demonstrating considerable variability across different examples. These observations raise critical concerns regarding the stability of DiT models, particularly for training efficiency and inference acceleration. We formally define the instability of DiT as Dynamic Feature Instability (DFI). We preliminary attribute these issues to the uncontrolled spectral norm $\sigma_{
m max}$ of DiT's Jacobians $J^{
m vanilla}$, which exponentially amplifies perturbations and destabilizes feature propagation. This aligns with findings in [43], where high spectral norms degrade model robustness and generalization capacity by amplifying input sensitivities, and mirrors the instability patterns observed in visual generative GAN training [19] without spectral normalization.

Training Convergence Comparison To validate the theoretical convergence rate in real implementations, we extend preliminary experiments recording the relationship between training steps and performance and FID[21] on ImageNet[7]. Both DiT models with/without LSCs are trained from scratch under identical settings. Results are revealed in Figure 4. The accelerated convergence of DiT w/ LSCs observed in

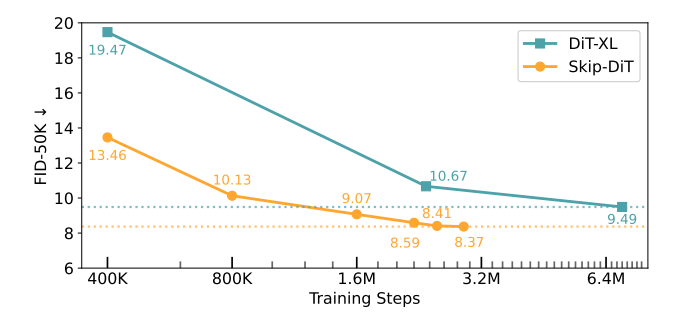


Figure 4. Training efficiency comparison between Skip-DiT and DiT-XL. Skip-DiT achieves superior FID-50K score on ImageNet at 1.6M training steps (vs. DiT-XL's 7M steps) and converges faster at 2.9M steps. Both models are evaluated on FID-50K under identical settings (no classifier-free guidance, cfg=1).

practical training demonstrates the training efficiency and model capability. This mirrors our theoretical analysis in Theorem 1, confirming that the spectral norm is effectively controlled with LSCs during training.

3.3. Integerating Long-Skip-Connection into DiT

To detail the DiT with Long-Skip-Connections(LSCs), we connect the shallow blocks to deep blocks with LSCs in DiT, named as Skip-DiT. Let \boldsymbol{x} denote the input noise embedding, and \boldsymbol{x}_l' represents the output at the l-th layer of Skip-DiT. The architecture consists of L sequential DiT blocks with LSCs. Each DiT block $\mathcal{F}_{\text{DiT}}^l$ at block l processes the features as $\boldsymbol{x}' = \mathcal{F}_{\text{DiT}}^l(\boldsymbol{x})$. The i-th skip branch l which can be denoted as $\mathcal{F}_{\text{Skip}}^i(\cdot,\cdot)$. Given output \boldsymbol{x}_l' from the start of the skip branch and \boldsymbol{x}_l' from the previous layer, the skip branch aggregates them to the input to l-th block as:

$$oldsymbol{x}_l = \mathcal{F}_{ ext{skin}}^i(oldsymbol{x}_i', oldsymbol{x}_{l-1}') = ext{Linear}(ext{Norm}(oldsymbol{x}_i' \oplus oldsymbol{x}_{l-1}'))$$
 (4)

where \oplus denotes concatenation, Norm represents the layer normalization, and Linear is a fully-connected layer. Each skip connection creates a shortcut path that helps preserve and process information from earlier layers, enabling better gradient flow and feature reuse throughout the network.

3.4. Spectral Analysis of Skip-Dit

Consider an ideal denoising diffusion transformer M with L identical blocks, where the denoising capability induces the following fundamental properties:

• Noise Reduction Invariance: Each transformer block \mathcal{T}_l strictly reduces noise magnitude of input h. This directly implies the Jacobian spectral norm (σ_{max}) constraint:

$$\sigma_{\max}\left(\frac{\partial \mathcal{T}_l}{\partial h}\right) \triangleq \gamma_l < 1$$
 (5)

• Transformer Blocks Homogeneity: Identical noise reduction ratio across layers $\gamma_l = \gamma, \quad \forall l \in \{1,...,L\}$. Thus, the complete model satisfies

$$\sigma_{\max}(M) = \prod_{l=1}^{L} \gamma = \gamma^{L} \ll 1 \tag{6}$$

Theorem 1. The spectral norm of the Jacobian matrix of DiT with Long-Skip-Connections is controlled more tightly than that of Vanilla DiT M, making the Skip-DiT model more robust, numerically stable, and capable of converging faster.

Proof. Define layer transformations for $L/2 < l \le L$ and their Jacobian matrices, where \mathcal{T} denotes the Transformer block and $0 < \alpha < 1$ denotes normlized concatetion:

$$h_{l+1}^{\text{vanilla}} = \mathcal{T}(h_l^{\text{vanilla}}), h_{l+1}^{\text{skip}} = (1-\alpha) \cdot \mathcal{T}(h_l^{\text{skip}}) + \alpha \cdot h_{L-l}^{\text{skip}}.$$

The corresponding Jacobian matrices J are:

$$J_{l}^{\text{vanilla}} = \frac{\partial \mathcal{T}\left(h_{l}\right)}{\partial h_{l}}, J_{l}^{\text{skip}} = (1 - \alpha) \cdot \frac{\partial \mathcal{T}\left(h_{l}\right)}{\partial h_{l}} + \alpha \cdot \frac{\partial h_{L-l}}{\partial h_{l}}.$$

Given $\gamma < 1$ and $2l - L \ge 1$ for $l \ge L/2$, the layer wise spectral norms σ_{max} of $M_{vanilla}$ and M_{skip} staisfy:

$$\sigma_{\max}(J_l^{\text{skip}}) \le (1 - \alpha)\gamma + \alpha\gamma^{2l-L} < \gamma = \sigma_{\max}(J_l^{\text{vanilla}})$$

For the full model Jacobian $J = \prod_{l=1}^{L} J_l$, the σ_{max} satisfy:

$$\sigma_{\max}(J^{\text{skip}}) < \prod_{l=0}^{L-1} \gamma = \gamma^L = \sigma_{\max}(J^{\text{vanilla}}).$$
 (7)

This spectral norm reduction attenuates perturbation growth through $\|\Delta h_L\| \leq (\sigma_{\max}(J))^L \|\Delta h_0\|$, stabilizes gradient flow via $\|\nabla_{\theta}\mathcal{L}\| \leq \sigma_{\max}(J) \|\nabla_{h_L}\mathcal{L}\|$, and improves the Lipschitz constant $\mathrm{Lip}(M_{\mathrm{skip}}) < \mathrm{Lip}(M_{\mathrm{vanilla}})$ with tight upper bound. This theoretical analysis aligns with our findings in Section 3.2, where Skip-DiT are proven to be more feature stable and training efficient through comprehensive visualizations and preliminary experiments.

3.5. Cached Inference Mechanism

The feature stability and robustness in Skip-DiT enables effective reuse of intermediate features across timesteps during denoising. To quantify this advantage, we analyze the similarity of transformer block outputs with versus without caching in both vanilla DiT and Skip-DiT.

Caching Strategy for Skip-DiT For Skip-DiT, we implement a hybrid caching strategy combining skip-connection-based block skipping from DeepCache [17], phased denoising strategy[13, 47], and errors accumulation guidance[11, 16] with errors predicted through static error records \mathcal{R} averaged from history. We identify the dynamic phase \mathcal{P} with static feature analysis before caching. The detailed caching algorithm is presented in Algorithm 1.

Visualizing Caching Stability . As visualized in Figure 3, Skip-DiT exhibits significantly higher feature similarity and smaller variance among examples compared to vanilla DiT, which employs FORA [30] and FasterDiffusion designed for DiT models. This demonstrates superior stability for cached inference. We attribute this improvement to the inherent feature stabilization and enhanced robustness. The latter can be theoretically grounded on M defined in sec.3.4:

Theorem 2. Under feature reuse with interval τ , Skip-DiT achieves tighter perturbation bounds than Vanilla DiT, enabling larger allowable reuse intervals while maintaining error tolerance ϵ_{\max} .

Proof. Let h_t be the reused feature with error ϵ_t , δ the perturbation bound per step, x the input, and θ the model parameters. Through the differential mean-value theorem and error propagation:

$$\epsilon_{t+1} = ||h_{t+1} - h_t|| \le \operatorname{Lip}(M)\epsilon_t + \delta$$

From Theorem 1, the Lipschitz constants and perturbation bounds satisfy: $\operatorname{Lip}(M_{\operatorname{skip}}) < \operatorname{Lip}(M_{\operatorname{vanilla}})$ and $\delta_{\operatorname{skip}} < \delta_{\operatorname{vanilla}}$. For T-step feature reuse, the cumulative error is:

$$\epsilon_T \le \frac{\operatorname{Lip}(M)^T - 1}{\operatorname{Lip}(M) - 1} \delta$$
 (8)

Considering the conditions above, the maximal interval τ satisfies: $\epsilon_{\tau}^{skip} = \epsilon_{\tau}^{vanilla} < \epsilon_{max}$.

Solving this yields $\tau_{\rm skip} > \tau_{\rm vanilla}$ under identical $\epsilon_{\rm max}$, which demonstrate better robustness and tolerance to error of Skip-DiT.

4. Experiments

4.1. Implementation Details

Models To start with, we add Long-Skip-Connections (LSCs) in DiT-XL [22] on the class-to-image task to prove the training efficiency and feature stability of Skip-DiT. We employ Latte [18] as our base model in video generation and Hunyuan-DiT for text-to-image generation to further demonstrate the remarkable effectiveness of Skip-DiT and its caching efficiency. Latte consists of spatial and temporal transformer blocks, suitable for both class-to-video and text-to-video tasks. Hunyuan-DiT [14], the first text-to-image DiT model with skip connections, is designed for text-to-image tasks. All DiT models are integrated with LSCs to evaluate the performance in both video and image generation tasks following the guidance in Section.3.3 and explore techniques for integrating LSCs into a pre-trained DiT model.

Datasets For the class-to-image task, Skip-DiT is trained on 256×256 ImageNet [7], following the dataset used by DiT-XL. In the class-to-video task, Skip-DiT is

Table 1. Class-to-video generation performance. The definition of the cache step n follows that in Table 2. For the UCF101 task, the scheduler is 50-steps-DDIM, while for the remaining tasks is 250-steps-DDPM. Latency and speedup are calculated on one A100 GPU. The notation n=i represents cache interval N in Algorithm 1. We highlight Baseline DiT models in grey, and the best metrics in **bold**.

					~1						
Method	FVD (\dagger)	FID (↓)	FF FVD (↓)	FID (↓)	Sk FVD(↓)	y FID (↓)	FVD (↓)	aichi FID(↓)	FLOPs (T)	Latency (s)	Speedup
Latte	155.22	22.97	28.88	5.36	49.46	11.51	166.84	11.57	278.63	9.90	1.00×
Δ-DiT FORA	161.62 160.52	25.33 23.52	25.80 27.23	4.46 4.64	51.70 52.90	11.67 11.96	188.39 198.56	12.09 13.68	226.10 240.26	8.09 9.00	1.22× 1.10×
PAB ₂₃ PAB ₃₅	213.50 1176.57	30.96 93.30	58.15 863.18	5.94 128.34	96.97 573.72	16.38 55.66	274.90 828.40	16.05 42.96	233.87 222.90	7.63 7.14	1.30× 1.39×
					Skip-DiT	with Cache	1 Inference				
original	141.30	23.78	20.62	4.32	49.21	11.92	163.03	13.55	290.05	10.02	1.00×
n = 2 $n = 3$ $n = 4$ $n = 5$ $n = 6$	141.42 137.98 143.00 145.39 151.77	21.46 19.93 19.03 18.72 18.78	23.55 26.76 30.19 35.52 42.41	4.49 4.75 5.18 5.86 6.42	51.13 54.17 57.36 62.92 68.96	12.66 13.11 13.77 14.18 15.16	167.54 179.43 188.44 209.38 208.04	13.89 (0.34 ↑) 14.53 14.38 15.20 15.78	180.68 145.87 125.99 121.02 111.07	6.40 5.24 4.57 4.35 4.12	1.56× 1.91× 2.19× 2.30× 2.43 ×

Algorithm 1 Skip-DiT with Cached Inference

Input Initial state \boldsymbol{x}^t , model \mathcal{F} , cache interval N, global error ϵ , static error records $\mathcal{R}(\boldsymbol{x}_{t=1}^T)$, dynamic Phase \mathcal{P} . Output Generated sequence $\{\boldsymbol{x}^t\}_{t=1}^T$

```
1: Global Timestep t (Full Inference):
 2: \boldsymbol{x'}^t \leftarrow \mathcal{F}^{L-1} \circ \cdots \circ \mathcal{F}^1(\boldsymbol{x}^t)
 3: Cache feature: \mathcal{C}_{L-1}^t \leftarrow \boldsymbol{x'}^t

4: \boldsymbol{x}^{t-1} = \mathcal{F}^L(\boldsymbol{x}^t)
 5: for k = 1 to N - 1 do
           7:
 8:
            Maintain cache: \mathcal{C}_{L-1}^t \leftarrow \mathcal{C}_{L-1}^t
 9:
            Accumulate error: \epsilon \leftarrow \epsilon + \mathcal{R}(t-k)
10:
            if t - k - 1 \in \mathcal{P} \mid\mid \epsilon > threshold then
11:
                  \epsilon \leftarrow 0; Break
12:
            end if
13:
14: end for
15: t \leftarrow t - k - 1;
16: Back to Full Inference until: t < 0;
```

trained on four datasets: FaceForensics [28], SkyTime-lapse [39], UCF101 [34], and Taichi-HD [31]. Following the experimental settings in Latte, we extract 16-frame video clips from these datasets and resize all frames to a resolution of 256×256. For the text-to-video task, the original Latte is trained on Webvid-10M [1] and Vimeo-2M [36], comprising approximately 330k text-video pairs in total. Considering that the resolution of Webvid-10M is lower than 512×512, we only sample 330k text-video pairs from Vimeo-2M for training, with a resolution of 512×512 and 16 frames.

Training Details In the class-to-image task, the model is initialized randomly and aligns all the training settings with

DiT-XL. The detailed training settings can be found in the Appendix. For class-to-video tasks, we train all instances of Skip-DiT from scratch on all datasets. For text-to-video tasks, we propose a two-stage continual training strategy:

- Skip-Connections training: Latte with LSC is initialized
 with the weights of the original Latte, and the weight of
 LSCs is initialized randomly. At this stage, only the LSCs
 are trained. It only takes one day on 8 H100 GPUs.
- Overall training: With LSCs Fully trained, all other parameters are unfrozen to perform overall training. At this stage, Skip-DiT rapidly recovers its generation capability within two days and can generate content comparable to the original Latte with an extra three days of training.

All our training experiments are conducted on 8 H100 GPUs, video-image joint training strategy proposed by Ma et al. [18] is employed to enhance training stability.

4.2. Results on Video Generation Tasks

Evaluation Details Following previous works [11, 16, 50] and Latte, we evaluate text-to-video models using VBench [10], Peak Signal-to-Noise Ratio (PSNR), Learned Perceptual Image Patch Similarity (LPIPS) [45], and Structural Similarity Index Measure (SSIM) [37]. VBench is a comprehensive benchmark suite comprising 16 evaluation dimensions. PSNR is a widely used metric for assessing the quality of image reconstruction, LPIPS measures feature distances extracted from pre-trained networks, and SSIM evaluates structural information differences. For class-to-image tasks, we evaluate the similarity between generated and real videos using Fréchet Video Distance (FVD) [35] and Fréchet Inception Distance (FID) [21], following the evaluation guidelines of StyleGAN-V [44].

Class-to-video Generation We compare the quantitative performance of Latte and Skip-DiT on four class-to-video tasks, as shown in Table 1. Skip-DiT consistently outper-

Table 2. Text-to-video generation performance. Inference latency and flop	s are evaluated with 1 A100 GPU. The notation $n = i$ represents
cache interval N in Algorithm 1. Baseline DiT models are highlighted in	grey, and the best metrics are emphasized in bold .

Model	Method	VBench(%) ↑	PSNR ↑	LPIPS ↓	SSIM ↑	FLOPs (T)	Latency (s)	Speedup			
	original	76.14	-	-	-	1587.25	27.11	1.00×			
	T-GATE	75.68 (\(\psi 0.46 \)	22.78	0.19	0.78	1470.72	24.15	1.12×			
	FORA	76.06 (\(\psi 0.08 \))	22.93	0.14	0.79	1341.72	24.21	1.19×			
Latte	Δ -DiT	76.06 (\(\psi 0.08 \))	24.01	0.17	0.81	1274.36	21.40	1.27×			
Latte	PAB_{235}	73.77 (\\documes2.37)	19.18	0.27	0.66	1288.08	23.24	1.24×			
	PAB_{347}	71.11 (\\$5.03)	18.20	0.32	0.63	1239.35	22.23	1.29×			
	PAB_{469}	70.20 (\$\square\$5.94)	17.40	0.35	0.60	1210.11	21.60	1.33×			
	AdaCache	76.07 (\$\dagger\$0.07)	22.23	0.19	0.78	934.85	16.95	1.60×			
	TeaCache	76.03 (\$\du0.11)	23.05	0.17	0.80	862.52	15.75	1.72×			
	original	75.60	-	-	-	1648.13	28.72	1.00×			
		65% steps cached									
	n=2	75.51 (\(\psi 0.09 \))	29.52	0.06	0.89	1127.83	19.28	1.49×			
	n = 3	75.26 (\(\psi 0.34 \)	27.46	0.09	0.85	974.80	16.67	1.72×			
Skip-DiT	n = 4	74.73 (\$\dagger\$0.87)	25.97	0.13	0.81	882.98	15.12	1.90×			
				75% steps	cached						
	n=2	75.36 (\\$0.24)	26.02	0.10	0.84	1066.62	18.25	1.57×			
	n = 3	75.07 (\(\psi 0.53 \))	22.85	0.18	0.76	852.38	14.88	1.93×			
	n = 4	74.43 (\1.17)	22.08	0.22	0.73	760.56	13.03	$\textbf{2.20} \times$			

forms Latte in terms of FVD scores across all tasks while achieving comparable performance in FID scores, demonstrating its strong video generation capabilities. Furthermore, we observe that Skip-DiT with cached inference significantly outperforms other caching methods across most metrics, incurring only an average loss of 2.37 in the FVD score and 0.27 in the FID score while achieving a $1.56\times$ speedup.

Table 3. Class-to-image generation performance. Speedups are calculated on an H100 GPU with a sample batch size of 8. The definition of n=i is the same as other tables. The classifier-free guidance scale is set to 1.5. Skip-DiTis trained with 2.9M steps. We highlight baseline models in grey and the best metrics in **bold**.

Methods	FID ↓	sFID ↓	IS ↑	Precision%	Recall %	Speedup
			DiT-X	ΚL		
original	2.30	4.71	276.26	82.68	57.65	1.00×
FORA	2.45	5.44	265.94	81.21	58.36	1.57×
Delta-DiT	2.47	5.61	265.33	81.05	58.83	1.45×
		Skip-D	iT with C	Cached Inference	;	
original	2.29	4.58	281.81	82.88	57.53	1.00×
n = 2	2.31	4.76	277.51	82.52	58.06	1.46×
n = 3	2.40	4.98	272.05	82.14	57.86	$1.73 \times$
n = 4	2.54	5.31	267.34	81.60	58.31	1.93×

Text-to-video Generation Table 2 presents evaluation results on text-to-video models. Videos are generated using the prompts of VBench [10], which is considered a more generalized benchmark [10, 50, 51]. Compared with the original Latte, Skip-DiT achieves a comparable VBench score (75.60 vs. 76.14) with only six days of continual pre-training on 330k training samples. To demonstrate the superiority of the cached inference of Skip-DiT, we evaluate two caching settings: caching at timesteps $700 \rightarrow 50$ and $800 \rightarrow 50$ (out of 1000 timesteps in total). In both settings,

Skip-DiT achieves the highest speedup while maintaining superior scores in PSNR, LPIPS, and SSIM, with only a minor loss in VBench score.

4.3. Results on Image Generation Tasks

We extend Skip-DiT to the class-to-image task, where Skip-DiT exceeds DiT-XL with only around 23% of its training cost (1.6M training steps vs.7M), and we choose the Skip-DiT trained with 2.9M steps for evaluation. Hunyuan-DiT [14] is a powerful text-to-image DiT model featuring LSCs. However, its skip connections have not been fully explored to accelerate generation.

Evaluation Details To evaluate the generalization of the caching mechanism in Skip-DiT for text-to-image tasks, we use the zero-shot Fréchet Inception Distance (FID) on the MS-COCO [15] validation dataset by generating 30k images based on its prompts, following the guidelines of Hunyuan-DiT. Additionally, we also employ Peak Signal-to-Noise Ratio (PSNR), Learned Perceptual Image Patch Similarity (LPIPS), and Structural Similarity Index Measure (SSIM) to evaluate similarity. For the class-to-image task, we evaluate models on ImageNet [7] by generating 50k images, and calculating evaluation metrics used in Peebles and Xie [22].

Evaluation Results Table 4 comprehensively compares Hunyuan-DiT and various caching methods. Notably, our caching mechanism achieves a $2.09 \times$ speedup without any degradation in FID or CLIP scores. Furthermore, it outperforms all other caching methods in terms of PSNR, LPIPS, and SSIM scores, consistently maintaining the highest performance even with a $1.96 \times$ speedup. These findings under-

Table 4. Text-to-image generation performance. Latency and speedup are calculated on one A100 GPU. The notation $n=i$ represents cache
interval N in Algorithm 1. We highlight baseline DiT models (without caching) in grey, and the best metrics in bold .

Method	FID (↓)	CLIP (†)	PSNR (†)	LPIPS (↓)	SSIM (†)	FLOPs (T)	Latency (s)	Speedup
HunYuan-DiT	32.64	30.51	-	-	-	514.02	18.69	1.00
TGATE	32.71	30.64	16.80	0.24	0.61	378.94	13.21	1.41
Δ -Cache	28.35	30.35	16.56	0.21	0.65	362.67	13.58	1.38
FORA	31.21	30.53	19.58	0.14	0.75	330.68	13.20	1.42
			Skip-D	iT with Cached l	Inference			
n=2	31.30	30.52	22.09	0.10	0.84	348.24	12.76	1.46
n = 3	29.53	30.55	21.25	0.11	0.81	299.48	10.91	1.71
n = 4	27.49	30.55	20.55	0.13	0.78	270.22	10.02	1.87
n = 5	28.37	30.56	19.94	0.14	0.76	260.47	9.51	1.96
n = 6	27.21	30.71	19.18	0.18	0.70	240.96	8.96	2.09

Table 5. Ablation study on different timestep ranges for caching. Total timesteps is 1000. We only perform cache in Skip-DiT at caching timesteps. We highlight the best metrics in **bold**.

Caching Timestep	VBench (%) ↑	PSNR ↑	LPIPS ↓	SSIM ↑
700→50 950→300	75.51 75.48	29.52 20.58	0.06 0.23	0.89 0.73
800→50 900→50	75.36 75.24	26.02 22.13	0.10 0.19	0.84 0.76

Table 6. Compatibility of Skip-DiT with other caching methods. The performance or other caching methods on vanilla DiT are shown in the table 2. Obvious improvements can be seen especially in PAB. We highlight the best metrics in **bold**.

Method	Δ VBench (%) \downarrow	PSNR ↑	LPIPS ↓	SSIM ↑
T-GATE	0.44	24.09	0.16	0.78
Δ -DiT	0.12	22.64	0.17	0.79
FORA	0.22	23.26	0.16	0.79
PAB_{235}	1.81	19.92	0.29	0.68
PAB_{347}	3.52	18.98	0.34	0.65
PAB_{469}	3.96	18.02	0.37	0.62

score the robustness and adaptability of our caching mechanism to image generation tasks. The results on the class-to-image task shown in Table 3, Skip-DiT also achieve the least loss while maintaining higher speedup.

4.4. Ablation studies

Identify Dynamic Phase for Better Caching After incorporating LSCs into DiT, we can statically choose the timesteps for caching with feature stability, thus we can identify the dynamic phase by caching similarity shown in Figure 3. However, previous work has observed that the denoising process is split into different phases in U-Net diffusion models by Zhang et al. [46] and Li et al. [13], highlighting the hidden dynamic phases which may lead to better performance. A heat map visualizing inner feature dynamics within blocks is shown in Figure 5, and significant changes are observed in the early denoising phase. In Table 5, we further validate this observation: under equivalent throughput, caching in the later timesteps $(700 \rightarrow 50)$, outperforms caching in the earlier timesteps $(950 \rightarrow 300)$, achieving

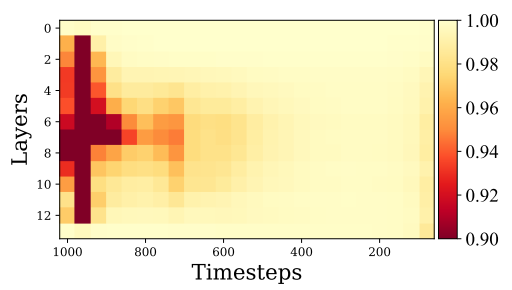


Figure 5. The feature dynamics of Latte with LSCs. Differences in features at the same layers across timesteps are evaluated.

superior PSNR, LPIPS, and SSIM scores. Additionally, we segmented the rapidly changing timesteps and experimented with additional caching ranges. All of these results show that increasing the ratio of the former phase significantly improves caching performance.

Compatibility of Skip-DiT with other caching methods

As shown in Table 6, we extend the existing text-to-video DiT caching methods to Skip-DiT and observe slight performance improvements. Taking PAB [50] as an example, it loses 1.15% less in VBench score and achieves noticeably better PSNR and SSIM scores on Skip-DiT compared to Latte, demonstrating the compatibility of Skip-DiT and that the stable features in Skip-DiT enhance the model robustness and caching efficiency.

5. Conclusion

In this work, we identify the *Dynamic Feature Instability* in vanilla DiT models and introduce Skip-DiT, a Long-Skip-Connections enhanced DiT model to produce more stable features and build training and inference efficient diffusion transformers. We designed a simpler but more efficient caching mechanism for Skip-DiT to improve inference efficiency in video and image generation tasks. By improving the stability of dynamic features, Skip-DiT unlocks the potential to cache most blocks while maintaining high generation quality. In addition, we guarantee stability and efficiency with theoretical analysis from the perspective of the spectral norm. Our proposed DiT achieves significant

speedup in training convergence and model capability. With the caching mechanism, we achieve maximum speedup in cache-based acceleration while maintaining the highest similarity to the original outputs. Furthermore, we identify the dynamic phase of Skip-DiT for a better caching strategy, demonstrating the effectiveness of caching. We also show that Skip-DiT is compatible with other caching methods, further extending its applicability. Overall, Skip-DiT can be seamlessly integrated with various DiT backbones, enabling real-time, high-quality video and image generation, while consistently outperforming baseline methods. We believe that Skip-DiT provides a simple yet powerful foundation for advancing future research and practical applications.

References

- [1] Max Bain, Arsha Nagrani, Gül Varol, and Andrew Zisserman. Frozen in time: A joint video and image encoder for end-to-end retrieval. In *Proceedings of the IEEE/CVF international conference on computer vision*, pages 1728–1738, 2021. 6
- [2] Fan Bao, Shen Nie, Kaiwen Xue, Yue Cao, Chongxuan Li, Hang Su, and Jun Zhu. All are worth words: A vit backbone for diffusion models. 2023 IEEE/CVF Conference on Computer Vision and Pattern Recognition (CVPR), pages 22669–22679, 2022. 3
- [3] James Betker, Gabriel Goh, Li Jing, † TimBrooks, Jianfeng Wang, Linjie Li, † LongOuyang, † JuntangZhuang, † JoyceLee, † YufeiGuo, † WesamManassra, † PrafullaDhariwal, † CaseyChu, † YunxinJiao, and Aditya Ramesh. Improving image generation with better captions. 1, 2
- [4] Junsong Chen, Jincheng Yu, Chongjian Ge, Lewei Yao, Enze Xie, Yue Wu, Zhongdao Wang, James T. Kwok, Ping Luo, Huchuan Lu, and Zhenguo Li. Pixart-α: Fast training of diffusion transformer for photorealistic text-to-image synthesis. ArXiv, abs/2310.00426, 2023. 1, 3
- [5] Lei Chen, Yuan Meng, Chen Tang, Xinzhu Ma, Jingyan Jiang, Xin Wang, Zhi Wang, and Wenwu Zhu. Q-dit: Accurate post-training quantization for diffusion transformers. arXiv preprint arXiv:2406.17343, 2024. 2
- [6] Pengtao Chen, Mingzhu Shen, Peng Ye, Jianjian Cao, Chongjun Tu, Christos-Savvas Bouganis, Yiren Zhao, and Tao Chen. Delta-dit: A training-free acceleration method tailored for diffusion transformers. arXiv preprint arXiv:2406.01125, 2024. 2, 3
- [7] Jia Deng, Wei Dong, Richard Socher, Li-Jia Li, Kai Li, and Li Fei-Fei. Imagenet: A large-scale hierarchical image database. In 2009 IEEE conference on computer vision and pattern recognition, pages 248–255. Ieee, 2009. 4, 5, 7, 2
- [8] Jonathan Ho, Ajay Jain, and Pieter Abbeel. Denoising diffusion probabilistic models. In Advances in Neural Information Processing Systems 33: Annual Conference on Neural Information Processing Systems 2020, NeurIPS 2020, December 6-12, 2020, virtual, 2020. 1, 3
- [9] Zhongzhan Huang, Pan Zhou, Shuicheng Yan, and Liang Lin. Scalelong: Towards more stable training of diffusion model

- via scaling network long skip connection. Advances in Neural Information Processing Systems, 36:70376–70401, 2023. 2, 3
- [10] Ziqi Huang, Yinan He, Jiashuo Yu, Fan Zhang, Chenyang Si, Yuming Jiang, Yuanhan Zhang, Tianxing Wu, Qingyang Jin, Nattapol Chanpaisit, Yaohui Wang, Xinyuan Chen, Limin Wang, Dahua Lin, Yu Qiao, and Ziwei Liu. Vbench: Comprehensive benchmark suite for video generative models. In Proceedings of the IEEE/CVF Conference on Computer Vision and Pattern Recognition (CVPR), pages 21807–21818, 2024. 6, 7, 2
- [11] Kumara Kahatapitiya, Haozhe Liu, Sen He, Ding Liu, Menglin Jia, Chenyang Zhang, Michael S Ryoo, and Tian Xie. Adaptive caching for faster video generation with diffusion transformers. *arXiv preprint arXiv:2411.02397*, 2024. 2, 3, 5, 6, 4
- [12] PKU-Yuan Lab and Tuzhan AI etc. Open-sora-plan, 2024. 3
- [13] Senmao Li, Taihang Hu, Fahad Shahbaz Khan, Linxuan Li, Shiqi Yang, Yaxing Wang, Ming-Ming Cheng, and Jian Yang. Faster diffusion: Rethinking the role of unet encoder in diffusion models. arXiv preprint arXiv:2312.09608, 2023. 1, 2, 3, 5, 8
- [14] Zhimin Li, Jianwei Zhang, Qin Lin, Jiangfeng Xiong, Yanxin Long, Xinchi Deng, Yingfang Zhang, Xingchao Liu, Minbin Huang, Zedong Xiao, Dayou Chen, Jiajun He, Jiahao Li, Wenyue Li, Chen Zhang, Rongwei Quan, Jianxiang Lu, Jiabin Huang, Xiaoyan Yuan, Xiaoxiao Zheng, Yixuan Li, Jihong Zhang, Chao Zhang, Meng Chen, Jie Liu, Zheng Fang, Weiyan Wang, Jinbao Xue, Yangyu Tao, Jianchen Zhu, Kai Liu, Sihuan Lin, Yifu Sun, Yun Li, Dongdong Wang, Mingtao Chen, Zhichao Hu, Xiao Xiao, Yan Chen, Yuhong Liu, Wei Liu, Di Wang, Yong Yang, Jie Jiang, and Qinglin Lu. Hunyuan-dit: A powerful multi-resolution diffusion transformer with fine-grained chinese understanding, 2024. 2, 5, 7, 3
- [15] Tsung-Yi Lin, Michael Maire, Serge J. Belongie, James Hays, Pietro Perona, Deva Ramanan, Piotr Dollár, and C. Lawrence Zitnick. Microsoft COCO: common objects in context. In Computer Vision - ECCV 2014 - 13th European Conference, Zurich, Switzerland, September 6-12, 2014, Proceedings, Part V, pages 740–755. Springer, 2014. 7
- [16] Feng Liu, Shiwei Zhang, Xiaofeng Wang, Yujie Wei, Haonan Qiu, Yuzhong Zhao, Yingya Zhang, Qixiang Ye, and Fang Wan. Timestep embedding tells: It's time to cache for video diffusion model. *arXiv preprint arXiv:2411.19108*, 2024. 2, 3, 5, 6, 4
- [17] Xinyin Ma, Gongfan Fang, and Xinchao Wang. Deepcache: Accelerating diffusion models for free. 2024 IEEE/CVF Conference on Computer Vision and Pattern Recognition (CVPR), pages 15762–15772, 2023. 2, 3, 5
- [18] Xin Ma, Yaohui Wang, Gengyun Jia, Xinyuan Chen, Ziwei Liu, Yuan-Fang Li, Cunjian Chen, and Yu Qiao. Latte: Latent diffusion transformer for video generation. arXiv preprint arXiv:2401.03048, 2024. 2, 3, 5, 6
- [19] Takeru Miyato, Toshiki Kataoka, Masanori Koyama, and Yuichi Yoshida. Spectral normalization for generative adversarial networks. In 6th International Conference on Learning Representations, ICLR 2018, Vancouver, BC, Canada, April

- 30 May 3, 2018, Conference Track Proceedings. OpenReview.net. 2018. 4
- [20] OpenAI. Sora: Creating video from text. https://openai.com/sora, 2024. 2, 3
- [21] Gaurav Parmar, Richard Zhang, and Jun-Yan Zhu. On buggy resizing libraries and surprising subtleties in FID calculation. *CoRR*, abs/2104.11222, 2021. 4, 6
- [22] William Peebles and Saining Xie. Scalable diffusion models with transformers. In *IEEE/CVF International Conference* on Computer Vision, ICCV 2023, Paris, France, October 1-6, 2023, pages 4172–4182. IEEE, 2023. 3, 5, 7, 2
- [23] William S. Peebles and Saining Xie. Scalable diffusion models with transformers. 2023 IEEE/CVF International Conference on Computer Vision (ICCV), pages 4172–4182, 2022. 1, 3
- [24] Dustin Podell, Zion English, Kyle Lacey, A. Blattmann, Tim Dockhorn, Jonas Muller, Joe Penna, and Robin Rombach. Sdxl: Improving latent diffusion models for high-resolution image synthesis. *ArXiv*, abs/2307.01952, 2023. 1, 2
- [25] Adam Polyak, Amit Zohar, Andrew Brown, Andros Tjandra, Animesh Sinha, Ann Lee, Apoorv Vyas, Bowen Shi, Chih-Yao Ma, Ching-Yao Chuang, David Yan, Dhruv Choudhary, Dingkang Wang, Geet Sethi, Guan Pang, Haoyu Ma, Ishan Misra, Ji Hou, Jialiang Wang, Kiran Jagadeesh, Kunpeng Li, Luxin Zhang, Mannat Singh, Mary Williamson, Matt Le, Matthew Yu, Mitesh Kumar Singh, Peizhao Zhang, Peter Vajda, Quentin Duval, Rohit Girdhar, Roshan Sumbaly, Sai Saketh Rambhatla, Sam Tsai, Samaneh Azadi, Samyak Datta, Sanyuan Chen, Sean Bell, Sharadh Ramaswamy, Shelly Sheynin, Siddharth Bhattacharya, Simran Motwani, Tao Xu, Tianhe Li, Tingbo Hou, Wei-Ning Hsu, Xi Yin, Xiaoliang Dai, Yaniv Taigman, Yaqiao Luo, Yen-Cheng Liu, Yi-Chiao Wu, Yue Zhao, Yuval Kirstain, Zecheng He, Zijian He, Albert Pumarola, Ali Thabet, Artsiom Sanakoyeu, Arun Mallya, Baishan Guo, Boris Araya, Breena Kerr, Carleigh Wood, Ce Liu, Cen Peng, Dimitry Vengertsev, Edgar Schonfeld, Elliot Blanchard, Felix Juefei-Xu, Fraylie Nord, Jeff Liang, John Hoffman, Jonas Kohler, Kaolin Fire, Karthik Sivakumar, Lawrence Chen, Licheng Yu, Luya Gao, Markos Georgopoulos, Rashel Moritz, Sara K. Sampson, Shikai Li, Simone Parmeggiani, Steve Fine, Tara Fowler, Vladan Petrovic, and Yuming Du. Movie Gen: A Cast of Media Foundation Models. arXiv e-prints, art. arXiv:2410.13720, 2024. 2, 3
- [26] Robin Rombach, A. Blattmann, Dominik Lorenz, Patrick Esser, and Björn Ommer. High-resolution image synthesis with latent diffusion models. 2022 IEEE/CVF Conference on Computer Vision and Pattern Recognition (CVPR), pages 10674–10685, 2021. 2
- [27] Olaf Ronneberger, Philipp Fischer, and Thomas Brox. U-net: Convolutional networks for biomedical image segmentation. *ArXiv*, abs/1505.04597, 2015. 1, 3
- [28] Andreas Rössler, Davide Cozzolino, Luisa Verdoliva, Christian Riess, Justus Thies, and Matthias Nießner. Faceforensics: A large-scale video dataset for forgery detection in human faces. *CoRR*, abs/1803.09179, 2018. 6
- [29] Axel Sauer, Dominik Lorenz, Andreas Blattmann, and Robin Rombach. Adversarial diffusion distillation. arXiv preprint arXiv:2311.17042, 2023. 2

- [30] Pratheba Selvaraju, Tianyu Ding, Tianyi Chen, Ilya Zharkov, and Luming Liang. Fora: Fast-forward caching in diffusion transformer acceleration. arXiv preprint arXiv:2407.01425, 2024. 1, 2, 4, 5
- [31] Aliaksandr Siarohin, Stéphane Lathuilière, Sergey Tulyakov, Elisa Ricci, and Nicu Sebe. First order motion model for image animation. In Advances in Neural Information Processing Systems 32: Annual Conference on Neural Information Processing Systems 2019, NeurIPS 2019, December 8-14, 2019, Vancouver, BC, Canada, pages 7135–7145, 2019. 6
- [32] Junhyuk So, Jungwon Lee, and Eunhyeok Park. Frdiff: Feature reuse for exquisite zero-shot acceleration of diffusion models. *arXiv preprint arXiv:2312.03517*, 2023. 3
- [33] Jiaming Song, Chenlin Meng, and Stefano Ermon. Denoising diffusion implicit models. In 9th International Conference on Learning Representations, ICLR 2021, Virtual Event, Austria, May 3-7, 2021. OpenReview.net, 2021. 2, 3
- [34] Khurram Soomro, Amir Roshan Zamir, and Mubarak Shah. UCF101: A dataset of 101 human actions classes from videos in the wild. *CoRR*, abs/1212.0402, 2012. 6
- [35] Thomas Unterthiner, Sjoerd van Steenkiste, Karol Kurach, Raphaël Marinier, Marcin Michalski, and Sylvain Gelly. Towards accurate generative models of video: A new metric & challenges. CoRR, abs/1812.01717, 2018. 6
- [36] Yaohui Wang, Xinyuan Chen, Xin Ma, Shangchen Zhou, Ziqi Huang, Yi Wang, Ceyuan Yang, Yinan He, Jiashuo Yu, Peiqing Yang, Yuwei Guo, Tianxing Wu, Chenyang Si, Yuming Jiang, Cunjian Chen, Chen Change Loy, Bo Dai, Dahua Lin, Yu Qiao, and Ziwei Liu. LAVIE: high-quality video generation with cascaded latent diffusion models. *CoRR*, abs/2309.15103, 2023. 6
- [37] Zhou Wang and Alan C. Bovik. A universal image quality index. *IEEE Signal Process. Lett.*, 9(3):81–84, 2002. 6
- [38] Felix Wimbauer, Bichen Wu, Edgar Schoenfeld, Xiaoliang Dai, Ji Hou, Zijian He, Artsiom Sanakoyeu, Peizhao Zhang, Sam Tsai, Jonas Kohler, et al. Cache me if you can: Accelerating diffusion models through block caching. In *Proceedings of the IEEE/CVF Conference on Computer Vision and Pattern Recognition*, pages 6211–6220, 2024. 3
- [39] Wei Xiong, Wenhan Luo, Lin Ma, Wei Liu, and Jiebo Luo. Learning to generate time-lapse videos using multi-stage dynamic generative adversarial networks. In 2018 IEEE Conference on Computer Vision and Pattern Recognition, CVPR 2018, Salt Lake City, UT, USA, June 18-22, 2018, pages 2364–2373. Computer Vision Foundation / IEEE Computer Society, 2018. 6
- [40] Zhuoyi Yang, Jiayan Teng, Wendi Zheng, Ming Ding, Shiyu Huang, Jiazheng Xu, Yuanming Yang, Wenyi Hong, Xiaohan Zhang, Guanyu Feng, et al. Cogvideox: Text-to-video diffusion models with an expert transformer. arXiv preprint arXiv:2408.06072, 2024. 3
- [41] Jingfeng Yao, Cheng Wang, Wenyu Liu, and Xinggang Wang. Fasterdit: Towards faster diffusion transformers training without architecture modification. *Advances in Neural Informa*tion Processing Systems, 37:56166–56189, 2025. 2, 4
- [42] Tianwei Yin, Michaël Gharbi, Richard Zhang, Eli Shechtman, Fredo Durand, William T Freeman, and Taesung Park.

- One-step diffusion with distribution matching distillation. In *Proceedings of the IEEE/CVF Conference on Computer Vision and Pattern Recognition*, pages 6613–6623, 2024. 2
- [43] Yuichi Yoshida and Takeru Miyato. Spectral norm regularization for improving the generalizability of deep learning. *CoRR*, abs/1705.10941, 2017. 4
- [44] Sihyun Yu, Jihoon Tack, Sangwoo Mo, Hyunsu Kim, Junho Kim, Jung-Woo Ha, and Jinwoo Shin. Generating videos with dynamics-aware implicit generative adversarial networks. In *International Conference on Learning Representations*, 2022.
- [45] Richard Zhang, Phillip Isola, Alexei A Efros, Eli Shechtman, and Oliver Wang. The unreasonable effectiveness of deep features as a perceptual metric. In *Proceedings of the IEEE* conference on computer vision and pattern recognition, pages 586–595, 2018. 6
- [46] Wentian Zhang, Haozhe Liu, Jinheng Xie, Francesco Faccio, Mike Zheng Shou, and Jürgen Schmidhuber. Cross-attention makes inference cumbersome in text-to-image diffusion models. CoRR, abs/2404.02747, 2024. 2, 8
- [47] Wentian Zhang, Haozhe Liu, Jinheng Xie, Francesco Faccio, Mike Zheng Shou, and Jürgen Schmidhuber. Cross-attention makes inference cumbersome in text-to-image diffusion models. arXiv preprint arXiv:2404.02747, 2024. 3, 5
- [48] Yiming Zhang, Zhening Xing, Yanhong Zeng, Youqing Fang, and Kai Chen. Pia: Your personalized image animator via plug-and-play modules in text-to-image models. In *Proceedings of the IEEE/CVF Conference on Computer Vision and Pattern Recognition*, pages 7747–7756, 2024. 1
- [49] Wangbo Zhao, Yizeng Han, Jiasheng Tang, Kai Wang, Yibing Song, Gao Huang, Fan Wang, and Yang You. Dynamic diffusion transformer. arXiv preprint arXiv:2410.03456, 2024. 2, 3
- [50] Xuanlei Zhao, Xiaolong Jin, Kai Wang, and Yang You. Realtime video generation with pyramid attention broadcast, 2024. 2, 3, 6, 7, 8, 4
- [51] Zangwei Zheng, Xiangyu Peng, Tianji Yang, Chenhui Shen, Shenggui Li, Hongxin Liu, Yukun Zhou, Tianyi Li, and Yang You. Open-sora: Democratizing efficient video production for all, 2024. 3, 7

Towards Stabilized and Efficient Diffusion Transformers through Long-Skip-Connections with Spectral Constraints

Supplementary Material

6. Detailed Proof of Theorems

Consider an ideal denoising diffusion transformer M with L identical blocks, where the denoising capability induces the following fundamental properties:

• Noise Reduction Invariance: Each transformer block \mathcal{T}_l strictly reduces noise magnitude of input h. This directly implies the Jacobian spectral norm (σ_{max}) constraint:

$$\sigma_{\max}\left(\frac{\partial \mathcal{T}_l}{\partial h}\right) \triangleq \gamma_l < 1$$
 (9)

• Transformer Blocks Homogeneity: Identical noise reduction ratio across layers $\gamma_l = \gamma, \quad \forall l \in \{1,...,L\}$. Thus, the complete model satisfies

$$\sigma_{\max}(M) = \prod_{l=1}^{L} \gamma = \gamma^{L} \ll 1 \tag{10}$$

6.1. Theorem1

The spectral norm of the Jacobian matrix of DiT with Long-Skip-Connections is controlled tighter than that of Vanilla DiT M, making the Skip-DiT model more robust, numerically stable, and capable of converging faster.

Proof. Define layer transformations for $L/2 < l \le L$ and their Jacobian matrices, where \mathcal{T} denotes the Transformer block and $0 < \alpha < 1$:

$$h_{l+1}^{\text{vanilla}} = \mathcal{T}(h_l^{\text{vanilla}}), h_{l+1}^{\text{skip}} = (1-\alpha) \cdot \mathcal{T}(h_l^{\text{skip}}) + \alpha \cdot h_{L-l}^{\text{skip}}.$$

The corresponding Jacobian matrices J are:

$$J_{l}^{\text{vanilla}} = \frac{\partial \mathcal{T}\left(h_{l}\right)}{\partial h_{l}}, J_{l}^{\text{skip}} = (1 - \alpha) \cdot \frac{\partial \mathcal{T}\left(h_{l}\right)}{\partial h_{l}} + \alpha \cdot \frac{\partial h_{L-l}}{\partial h_{l}}.$$

Applying subadditivity and submultiplicativity of spectral norms σ_{max} :

$$\sigma_{\max}(J_l^{\text{skip}}) \le (1 - \alpha)\gamma + \alpha\gamma^{2l - L}.$$
 (11)

Given $\gamma < 1$ and $2l - L \ge 1$ for l > L/2, we establish the layer-wise bound:

$$\sigma_{\max}(J_l^{\text{skip}}) < \gamma = \sigma_{\max}(J_l^{\text{vanilla}}).$$
 (12)

For the full model Jacobian $J = \prod_{l=1}^{L} J_l$, the spectral norms satisfy:

$$\sigma_{\max}(J^{\text{skip}}) \le \prod_{l=0}^{L-1} \left[(1-\alpha)\gamma + \alpha\gamma^{2l-L} \right]$$

$$< \prod_{l=0}^{L-1} \gamma = \gamma^{L} = \sigma_{\max}(J^{\text{vanilla}}). \tag{13}$$

This spectral radius reduction attenuates perturbation growth through $\|\delta h_L\| \leq (\sigma_{\max}(J))^L \|\delta h_0\|$, stabilizes gradient flow via $\|\nabla_{\theta}\mathcal{L}\| \leq \sigma_{\max}(J) \|\nabla_{h_L}\mathcal{L}\|$, and improves the Lipschitz constant $\operatorname{Lip}(M_{\operatorname{skip}}) < \operatorname{Lip}(M_{\operatorname{vanilla}})$.

6.2. Theorem2

Under feature reuse with interval τ , Skip-DiT achieves tighter perturbation bounds than Vanilla DiT, enabling larger allowable reuse intervals while maintaining error tolerance $\epsilon_{\rm max}$

Proof. Let h_t be the reused feature with error ϵ_t , δ the perturbation bound per step, x the input, and θ the model parameters. Through the differential mean-value theorem and error propagation:

$$||f(x; \theta + \Delta \theta) - f(x; \theta)|| \le \sup_{\theta'} \left\| \frac{\partial f}{\partial \theta} \right\| ||\Delta \theta|| \triangleq \delta$$
 (14)

$$\epsilon_{t+1} = ||h_{t+1} - h_t|| \le \operatorname{Lip}(M)\epsilon_t + \delta \tag{15}$$

From Theorem 1, the Lipschitz constants satisfy:

$$\operatorname{Lip}(M_{\operatorname{skip}}) = \sigma_{\max}(J^{\operatorname{skip}}) < \gamma^L = \operatorname{Lip}(M_{\operatorname{vanilla}})$$
 (16)

The perturbation bounds inherit:

$$\delta_{\text{skip}} = C_{\text{skip}} \|\Delta\theta\| < C_{\text{vanilla}} \|\Delta\theta\| = \delta_{\text{vanilla}}$$
 (17)

where C. bounds the parameter-to-output Jacobian.

$$\left\| \frac{\partial f_{\text{skip}}}{\partial \theta} \right\| = \left\| \prod_{l=1}^{L} \frac{\partial h_{l}}{\partial \theta} \right\| \leq \prod_{l=1}^{L} \left\| \frac{\partial h_{l}}{\partial \theta} \right\|$$

$$= \prod_{l=1}^{L} \left[(1 - \alpha)\gamma + \alpha \gamma^{2l - L} \right] \cdot C_{\text{base}}$$

$$< \prod_{l=1}^{L} \gamma \cdot C_{\text{base}} = C_{\text{vanilla}}$$

For T-step feature reuse, cumulative error develops as:

$$\epsilon_T \le \frac{\operatorname{Lip}(M)^T - 1}{\operatorname{Lip}(M) - 1} \delta$$
(18)

Given $\sigma_{\max}(J^{\text{skip}}) < \gamma^L$ and $\delta_{\text{skip}} < \delta_{\text{vanilla}}$, the maximal interval τ satisfies:

$$\frac{\sigma_{\max}(J^{\text{skip}})^{\tau} - 1}{\sigma_{\max}(J^{\text{skip}}) - 1} \delta_{\text{skip}} = \frac{\gamma^{L\tau} - 1}{\gamma^{L} - 1} \delta_{\text{vanilla}} = \epsilon_{\max} \quad (19)$$

Solving equation 19 yields $\tau_{\rm skip} > \tau_{\rm vanilla}$ under identical $\epsilon_{\rm max}$, proving Skip-DiT permits larger reuse intervals.

Table 7. Comparison of training efficiency between DiT-XL and Skip-DiT. Images are generated with a 250-step DDPM solver. The term cfg refers to classifier-free guidance scales, where metrics for cfg=1.0 are computed without classifier-free guidance. The best metrics are highlighted in **bold**. Skip-DiT significantly exceeds DiT-XL/2 with much less training steps.

Model	Steps	FID ↓	sFID ↓	IS ↑	Precision ↑	Recall ↑
DiT-XL/2	7000k	9.49	7.17	122.49	0.67	0.68
Skip-DiT	400k 800k 1600k 2200k 2500k 2900k	13.46 10.13 9.07 8.59 8.41 8.37	5.83 5.87 6.26 6.41 6.30 6.50	87.45 108.28 119.38 124.74 125.16 127.63	0.67 0.68 0.68 0.68 0.68 0.68	0.63 0.65 0.67 0.67 0.67 0.68

7. Class-to-image Generation Experiments

Peebles and Xie [22] proposed the first diffusion model based on the transformer architecture, and it outperforms all prior diffusion models on the class conditional ImageNet [7] 512×512 and 256×256 benchmarks. We add skip connections to its largest model, DiT-XL, to get Skip-DiT. We train Skip-DiT on class conditional ImageNet with resolution 256×256 from scratch with completely the same experimental settings as DiT-XL, and far exceeds DiT-XL with only around 38% of its training cost.

Training of Skip-DiT We add long-skip-connections in DiT-XL and train Skip-DiT for 2.9M steps on 8 A100 GPUs, compared to 7M steps for DiT-XL, which also uses 8 A100 GPUs. The datasets and other training settings remain identical to those used for DiT-XL, and we utilize the official training code of DiT-XL[†]. The performance comparison is presented in Table 7, which demonstrates that Skip-DiT significantly outperforms DiT-XL while requiring only 23% of its training steps (1.6M vs. 7M), highlighting the training efficiency and effectiveness of Skip-DiT.

Accelerating Evaluation We evaluate Skip-DiT and compare its performance against two other caching methods: Δ -DiT and FORA. As shown in Table 8, Skip-DiT achieves a 1.46× speedup with only a minimal FID loss of 0.02 when the classifier-free guidance scale is set to 1.5, compared to the 7–8× larger losses observed with Δ -DiT and FORA. Moreover, even with a 1.9× acceleration, Skip-DiT performs better than the other caching methods. These findings further confirm the effectiveness of Skip-DiT for class-to-image tasks.

8. Evaluation Details

VBench [10] is a novel evaluation framework for video generation models. It breaks down video generation assess-

Table 8. Class-to-image generation performance. The definition of the cache step n follows that in Table 4. Images are generated with a 250-step DDPM solver. Speedups are calculated on an H100 GPU with a sample batch size of 8. n=i indicates caching the high-level features in x_t for reuse during the inference of $x_{t-1}, x_{t-2}, \ldots, x_{t-n+1}$. The term cfg refers to classifier-free guidance scales, where metrics for cfg=1.0 are computed without classifier-free guidance. We highlight baseline DiT models (without caching) in grey and the best metrics in **bold**.

Methods	FID ↓	sFID ↓	IS ↑	Precision%	Recall%	Cnoodun			
Methods	FID ↓	SFID ↓	15 1	Precision%	Recair%	Speedup			
cfg=1.5									
DiT-XL	2.30	4.71	276.26	82.68	57.65	1.00×			
FORA	2.45	5.44	265.94	81.21	58.36	1.57×			
Delta-DiT	2.47	5.61	265.33	81.05	58.83	1.45×			
Faster-Diff	4.96	10.19	223.21	75.21	59.28	$1.42 \times$			
Skip-DiT with Cached Inference									
Skip-DiT	2.29	4.58	281.81	82.88	57.53	1.00×			
n = 2	2.31	4.76	277.51	82.52	58.06	1.46×			
n = 3	2.40	4.98	272.05	82.14	57.86	1.73×			
n = 4	2.54	5.31	267.34	81.60	58.31	1.93×			
			cfg=1.	0					
DiT-XL	9.49	7.17	122.49	66.66	67.69	1.00×			
FORA	11.72	9.27	113.01	64.46	67.69	1.53×			
Delta-DiT	12.03	9.68	111.86	64.57	67.53	1.42×			
Faster-Diff	22.98	18.09	80.41	56.53	67.41	1.42×			
Skip-DiT with Cached Inference									
Skip-DiT	8.37	6.50	127.63	68.06	67.89	1.00×			
n = 2	9.25	7.09	123.57	67.32	67.40	1.46×			
n = 3	10.18	7.72	119.60	66.53	67.84	$1.71 \times$			
n = 4	11.37	8.49	116.01	65.73	67.32	1.92×			

ment to 16 dimensions from video quality and condition consistency: subject consistency, background consistency, temporal flickering, motion smoothness, dynamic degree, aesthetic quality, imaging quality, object class, multiple objects, human action, color, spatial relationship, scene, temporal style, appearance style, overall consistency.

Peak Signal-to-Noise Ratio (PSNR) measures generated visual content quality by comparing a processed version \mathbf{v} to the original reference \mathbf{v}_r by:

$$PSNR = 10 \times \log_{10}\left(\frac{R^2}{MSE(\mathbf{v}, \mathbf{v}_r)}\right)$$
 (20)

where R is the maximum possible pixel value, and $MSE(\cdot,\cdot)$ calculates the Mean Squared Error between original and processed images or videos. Higher PSNR indicates better reconstruction quality. However, PSNR does not always correlate with human perception and is sensitive to pixel-level changes.

Structural Similarity Index Measure (SSIM) is a perceptual metric that evaluates image quality by considering luminance, contrast, and structure:

SSIM =
$$[l(\mathbf{v}, \mathbf{v}_r)]^{\alpha} \cdot [c(\mathbf{v}, \mathbf{v}_r)]^{\beta} \cdot [s(\mathbf{v}, \mathbf{v}_r \mathbf{v}_r)]^{\gamma}$$
 (21)

[†]https://github.com/facebookresearch/DiT

where α, β, γ are weights for luminance, contrast, and structure quality, where luminance comparison is $l(x,y) = \frac{2\mu_{\mathbf{v}}\mu_{\mathbf{v}_r} + C_1}{\mu_{\mathbf{v}}^2 + \mu_{\mathbf{v}_r}^2 + C_1}$, contrast comparison is $c(x,y) = \frac{2\sigma_{\mathbf{v}}\sigma_{\mathbf{v}_r} + C_2}{\sigma_{\mathbf{v}}^2 + \sigma_{\mathbf{v}_r}^2 + C_2}$, and structure comparison is $s(x,y) = \frac{\sigma_{xy} + C_3}{\sigma_{\mathbf{v}}\sigma_{\mathbf{v}_r} + C_3}$, with C denoting numerical stability coefficients. SSIM scores range from -1 to 1, where 1 means identical visual content.

Learned Perceptual Image Patch Similarity (LPIPS) is a deep learning-based metric that measures perceptual similarity using L2-Norm of visual features $v \in \mathbb{R}^{H \times W \times C}$ extracted from pretrained CNN $\mathcal{F}(\cdot)$. LPIPS captures semantic similarities and is therefore more robust to small geometric transformations than PSNR and SSIM.

LPIPS =
$$\frac{1}{HW} \sum_{h,w} ||\mathcal{F}(v_r) - \mathcal{F}(v)||_2^2$$
 (22)

Fréchet Inception Distance (FID) and Fréchet Video Distance (FVD) FID measures the quality and diversity of generated images by computing distance between feature distributions of reference $\mathcal{N}(\mu_r, \Sigma_r)$ and generated images $\mathcal{N}(\mu, \Sigma)$ using inception architecture CNNs, where μ, Σ are mean and covariance of features.

$$FID = ||\mu_r - \mu||^2 + Tr(\Sigma_r + \Sigma - 2(\Sigma_r \Sigma)^{1/2})$$
 (23)

FVD is a video extension of FID. Lower FID and FVD indicate higher generation quality.

Table 9. Comparison of our caching method with the faster sampler DDIM. Skip-Cache is evaluated with a 250-steps DDPM and compared to the DDIM sampler under similar throughput. Baseline DiT models (without caching) are highlighted in grey , and the best metrics are indicated in **bold**. Notably, DDIM outperforms the 250-step DDPM in the UCF101 task for both Latte and Skip-DiT. Skip-Cache denotes Skip-DiT with cached inference.

Method	UCF: FVD↓		FF FVD↓			y FID↓	Tai FVD↓	
Latte Skip-DiT	165.04 173.70	23.75 22.95	28.88 20.62	5.36 4.32	49.46 49.22	11.51 12.05	166.84 163.03	
Skip-DiT _{n=2} DDIM+Skip-DiT DDIM+Latte	165.60 134.22 146.78		23.55 37.28 39.10	4.49 6.48 6.47	51.13 86.39 78.38	13.67	167.54 343.97 321.97	21.01
Skip-DiT _{n=3} DDIM+Skip-DiT DDIM+Latte	169.37 139.52 148.46	24.71	26.76 39.20 41.00	4.75 6.49 6.54	54.17 90.62 74.39	13.80	179.43 328.47 327.22	14.53 21.33 22.96

9. Scheduler Selection for text-to-video Tasks

For the text-to-video generation task, all the videos generated for evaluation are sampled with 50 steps DDIM [33], which is the default setting used in Latte. In the class-to-video generation tasks, vanilla Latte uses 250-step DDPM [8] as

the default solver for class-to-video tasks, which we adopt for all tasks except UCF101. For UCF101, we employ 50-step DDIM [33], as it outperforms 250-step DDPM on both Latte and Skip-DiT. Table 9 highlights this phenomenon, showing our methods consistently outperform DDPM-250 under comparable throughput, except for UCF101, where DDIM performs better than 250 steps DDPM. In the text-to-image task, we choose 50-step DDIM for sampling, and for class-to-image task, we choose 25-steps DDPM.

10. Implementation of Other Caching Methods

DeepCache DeepCache [17] is a training-free caching method designed for U-Net-based diffusion models, leveraging the inherent temporal redundancy in sequential denoising steps. It utilizes the skip connections of the U-Net to reuse high-level features while updating low-level features efficiently. Skip-DiT shares significant similarities with DeepCache but extends the method to DiT models. Specifically, we upgrade traditional DiT models to Skip-DiT and cache them using Skip-DiT. In the work of DeepCache, two key caching decisions are introduced: (1) N: the number of steps for reusing cached high-level features. Cached features are computed once and reused for the next N-1 steps. (2) The layer at which caching is performed. For instance, caching at the first layer ensures that only the first and last layers of the U-Net are recomputed. In Skip-DiT, we adopt these two caching strategies and additionally account for the timesteps to cache, addressing the greater complexity of DiT models compared to U-Net-based diffusion models. For all tasks except the class-to-image task, caching is performed at the first layer, whereas for the class-to-image task, it is applied at the third layer.

 $\Delta ext{-DiT}$ $\Delta ext{-DiT}$ [6] is a training-free caching method designed for image-generating DiT models. Instead of caching the feature maps directly, it uses the offsets of features as cache objects to preserve input information. This approach is based on the observation that the front blocks of DiT are responsible for generating the image outlines, while the rear blocks focus on finer details. A hyperparameter b is introduced to denote the boundary between the outline and detail generation stages. When $t \leq b$, $\Delta ext{-Cache}$ is applied to the rear blocks; when t > b, it is applied to the front blocks. The number of cached blocks is represented by N_c .

While this caching method was initially designed for image generation tasks, we extend it to video generation tasks. In video generation, we observe significant degradation in performance when caching the rear blocks, so we restrict caching to the front blocks during the outline generation stage. For Hunyuan-DiT [14], we cache the middle blocks due to the U-shaped transformer architecture. Detailed configurations are provided in Table 10.

Table 10. Configuration details for Δ -Cache in different models and tasks. t2v denotes text-to-video, c2v denotes class-to-video, t2i denotes text-to-image, and c2i denotes class-to-image.

Δ-DiT	Task	Diffusion steps	b	All layers	N_c
Latte	t2v	50	12	28	21
Latte	c2v	250	60	14	10
Hunyuan	t2i	50	12	28	18
DiT-XL/2	c2i	250	60	28	21

PAB PAB (Pyramid Attention Broadcast) [50] is one of the most promising caching methods designed for real-time video generation. The method leverages the observation that attention differences during the diffusion process follow a U-shaped pattern, broadcasting attention outputs to subsequent steps in a pyramid-like manner. Different broadcast ranges are set for three types of attention—spatial, temporal, and cross-attention—based on their respective differences. $PAB_{\alpha\beta\gamma}$ denotes the broadcast ranges for spatial (α) , temporal (β) , and cross (γ) attentions.

In this work, we use the official implementation of PAB for text-to-video tasks on Latte and adapt the caching method to other tasks in-house. For the class-to-video task, where cross-attention is absent, $PAB_{\alpha\beta}$ refers to the broadcast ranges of spatial (α) and temporal (β) attentions. In the text-to-image task, which lacks temporal attention, $PAB_{\alpha\beta}$ instead denotes the broadcast ranges of spatial (α) and cross (β) attentions. We do not apply PAB to the class-to-image task, as it involves only spatial attention.

Table 11. Configuration details for T-GATE in different settings. *t2v* denotes text-to-video, *t2i* denotes text-to-image.

T-GATE	Task	Diffusion steps	m	k
Latte	t2v	50	20	2 2
Hunyuan-DiT	t2i	50	20	

T-Gates T-Gates divide the diffusion process into two phases: (1) the Semantics-Planning Phase and (2) the Fidelity-Improving Phase. In the first phase, self-attention is computed and reused every k step. In the second phase, cross-attention is cached using a caching mechanism. The hyperparameter m determines the boundary between these two phases. For our implementation, we use the same hyperparameters as PAB [50]. Detailed configurations are provided in Table 11.

FORA FORA (Fast-Forward Caching) [30] stores and reuses intermediate outputs from attention and MLP layers across denoising steps. However, in the original FORA paper, features are cached in advance before the diffusion process. We do not adopt this approach, as it is a highly time-consuming process. Instead, in this work, we skip the "Initialization" step in FORA and calculate the features dynamically during the diffusion process.

AdaCache AdaCache [11] identifies the feature sample-variance in the DiT, and proposes to predict the feature similarity of the current timestep to decide whether to cache. The codebook for Latte, which records the threshold is not released. We provide a version of codebook which almost reproduce the performance in the paper. The codebook is as follows: $\{0.08:3,0.10:2,0.12:1\}$

TeaCache Same as AdaCache, TeaCache[16] also discovers the feature instability in DiT. Different from AdaCache, TeaCache finds the relationship between input and output similarity and employ high-order polynomial functions to predict the similarity of the current timestep. We use the official codebase of it and choose the slow-caching strategy to evaluate its upper-bound.

11. Case Study

Video Generation In Figure 6, we showcase the generated video frames from text prompts with Skip-DiT, PAB, and comparing them to the original model. From generating portraits to scenery, Skip-DiT with caching consistently demonstrates better visual fidelity along with faster generation speeds. Figure 7 presents class-to-video generation examples with Skip-DiT with varying caching steps $\in \{2,4,6\}$. By comparing the output of Skip-DiT with cache to standard output, we see Skip-DiT maintains good generation quality across different caching steps.

Image Generation Figure 8 compares qualitative results of Skip-DiT compared to other caching-based acceleration methods (Δ -DiT, FORA, T-GATE) on Hunyuan-DiT. In Figure 9, Skip-DiT show distinct edges in higher speedup and similarity to the original generation, while other baselines exist with different degrees of change in details such as color, texture, and posture. Similarly, we present Skip-DiT with varying caching steps in Figure 9, showing that with more steps cached, it still maintains high fidelity to the original generation.

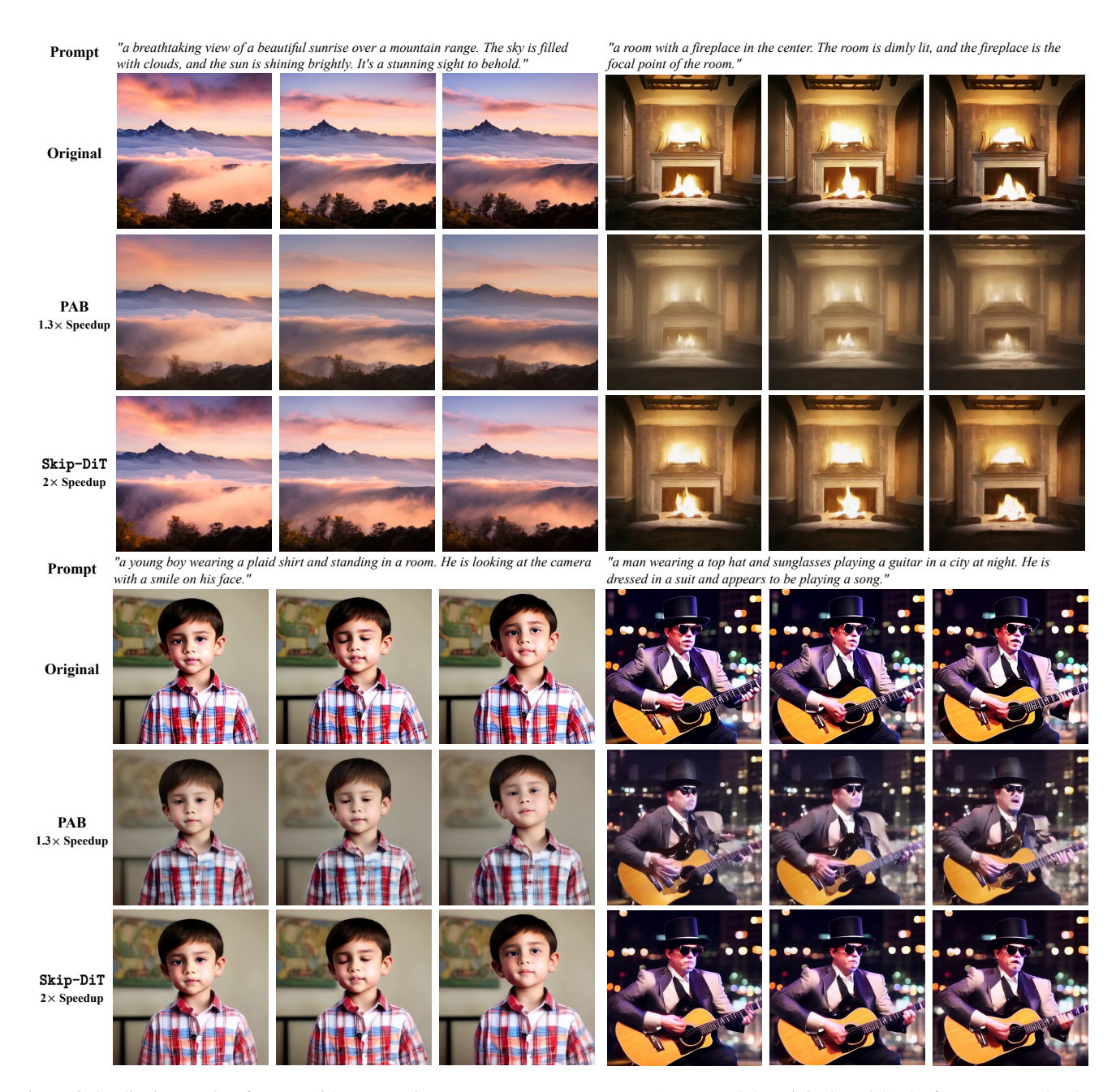


Figure 6. Qualitative results of text-to-video generation. We present Skip-DiT, PAB_{469} , and the original model. The frames are randomly sampled from the generated video.

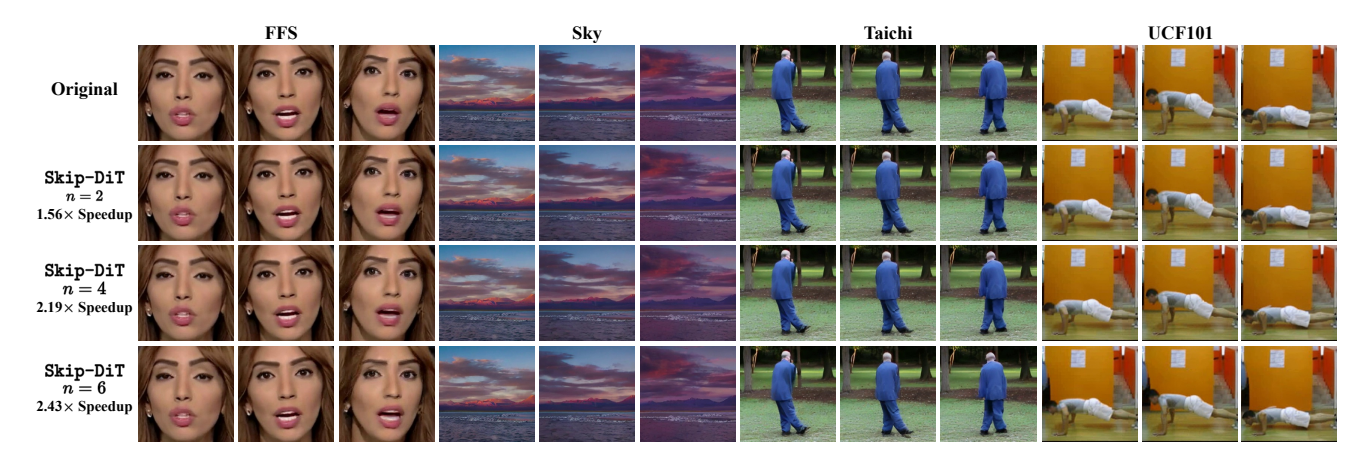


Figure 7. Qualitative results of class-to-video generation. We present the original video generation model and Skip-DiT with different caching steps n. The frames are randomly sampled from the generated video.



Figure 8. Qualitative results of text-to-image generation. We present Skip-DiT, Δ -DiT, FORA, T-GATE, and the original model.

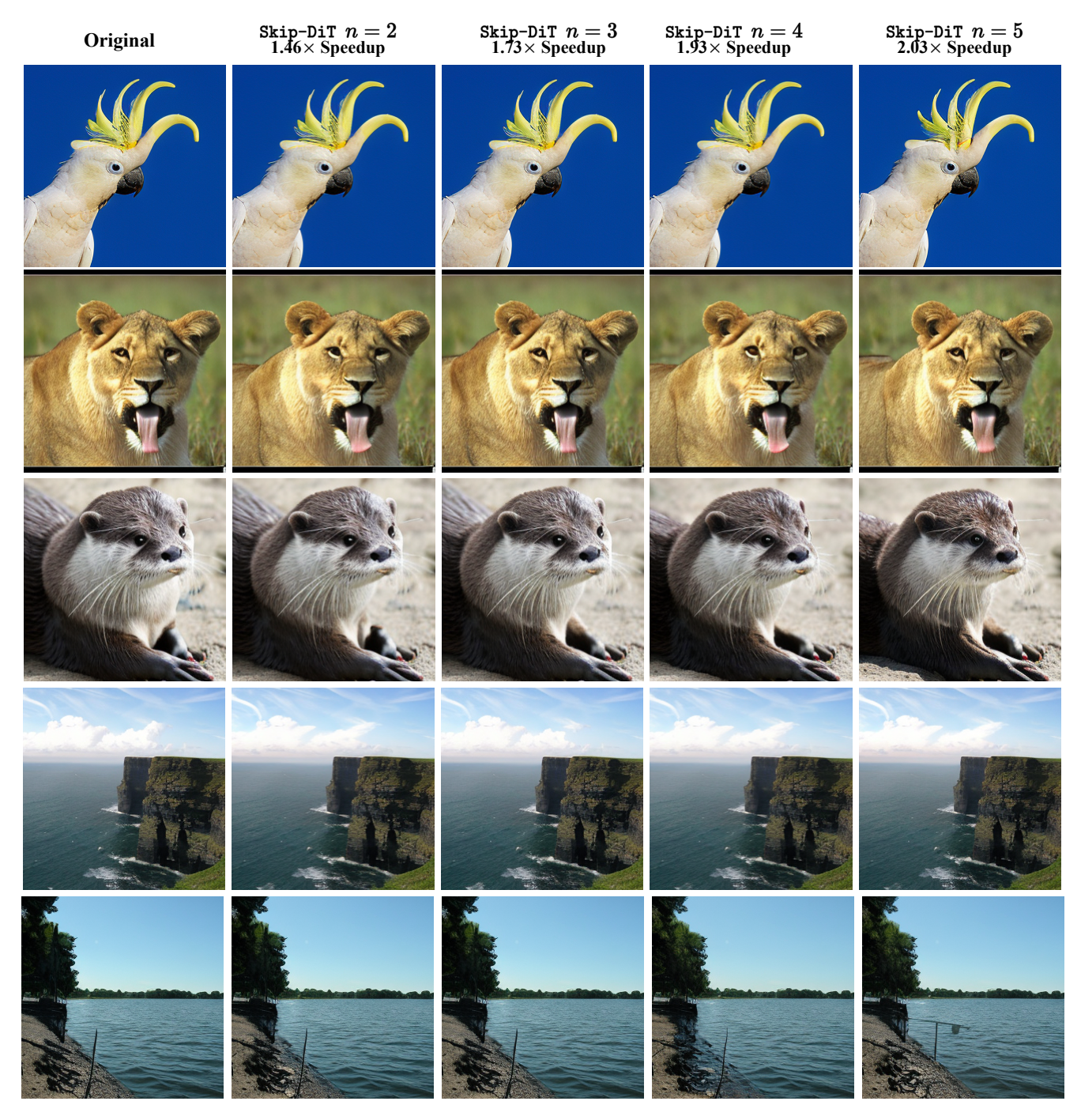


Figure 9. Qualitative results of class-to-image generation. We present the original image generation model and Skip-DiT with different caching steps n.